**Supplemental materials for:**

# Quality Carbon Fiber from Fractionated Lignin

Qiang Li[1,2], Shangxian Xie[1,2,3], Wilson K. Serem[4], Mandar T. Naik[5], Li Liu[6,7*], Joshua S. Yuan[1,2,3*]

[1]Texas A&M Agrilife Synthetic and Systems Biology Innovation Hub, Texas A&M University, College Station, TX 77843, USA

[2]Department of Plant Pathology and Microbiology, Texas A&M University, College Station, TX 77843, USA

[3]Institute for Plant Genomics and Biotechnology, Texas A&M University, College Station, TX 77843, USA

[4]Material Characterization Facility, Texas A&M University, College Station, TX 77843, USA

[5]Biomolecular NMR Laboratory, Department of Biochemistry and Biophysics, Texas A&M University, College Station, Texas 77843, USA

[6]Department of Chemistry, Texas A&M University, College Station, TX 77843, USA

[7]Department of Materials Science and Engineering, Texas A&M University, College Station, TX 77843, USA

*Corresponding: Li Liu, li.liu@tamu.edu; Joshua S. Yuan, syuan@tamu.edu

## Materials

Alkali Kraft lignin with low sulfonate content (370959), laccase (from *Trametes versicolor*, 0.5 U/mg, 38429), 1-hydroxy benzotriazolehydrate (HBT), *N,N*-dimethylformamide (DMF, 99.8%), and graphite (99% carbon basis) were purchased from Sigma–Aldrich, USA. Polyacrylonitrile (PAN, Mw = 150,000 g/mol) was purchased from Pfaltz & Bauer, USA.

## Enzymatic treatment of lignin

Kraft lignin (70 g) was added into a phosphate buffer (P-buffer, 0.2M, pH 7.0) to achieve a lignin concentration of 10 wt%. Laccase was then added into P-buffer with the loading of 15 mg/g lignin, and the HBT was used as mediator at 25 mg/g lignin. The treatment was carried out in a Biostat® A reactor (Sartorius, Bohemia, NY), with the oxygen flow rate at 5 ccm, temperature at 50 $^{o}$C, and the stirring speed at 200 rpm. After 48-hour of treatment, the mixture was separated by centrifugation at 25 000 g into water-insoluble and water-soluble fractions. Water-insoluble lignin fraction was then washed with 200 mL of deionized water for three times. Water-soluble lignin fraction was further precipitated into 500 mL of 2 M sulfuric acid and centrifuged again to render the solid phase. After centrifugation and lyophilization, the two fractions of lignin, namely insoluble lignin and soluble lignin, were obtained in powder form.

## $^{13}$C NMR Spectroscopy

All lignin samples were acetylated as described by Chen et al (1992)[1] for $^{13}$C NMR characterization. NMR spectra were acquired on an Avance III 500 with a HCN cryoprobe. The acetylated lignin (150 mg) was dissolved in 1 mL of DMSO-*d6* and placed in a 5-mm Wilmad NMR tube. Chromium (III) acetylacetone (0.01 M) was added into lignin solution as a relaxant.[2]

The methyl peak (39.5 ppm) of DMSO-*d6* was used as an internal reference. A 90 °C pulse width, a 1.2 s acquisition time, and a 1.0 s relaxation time were used. Data were collected with a total of 15000 scans. The $^{13}C$ NMR spectra were shown in Fig. S1, and the assignments of lignin functional groups were listed in Table S1. The integration of aromatic region (162-102 ppm) was set as 1, and the frequency of hydroxyl groups was integrated based on the aromatic region and presented as the number per aromatic ring.

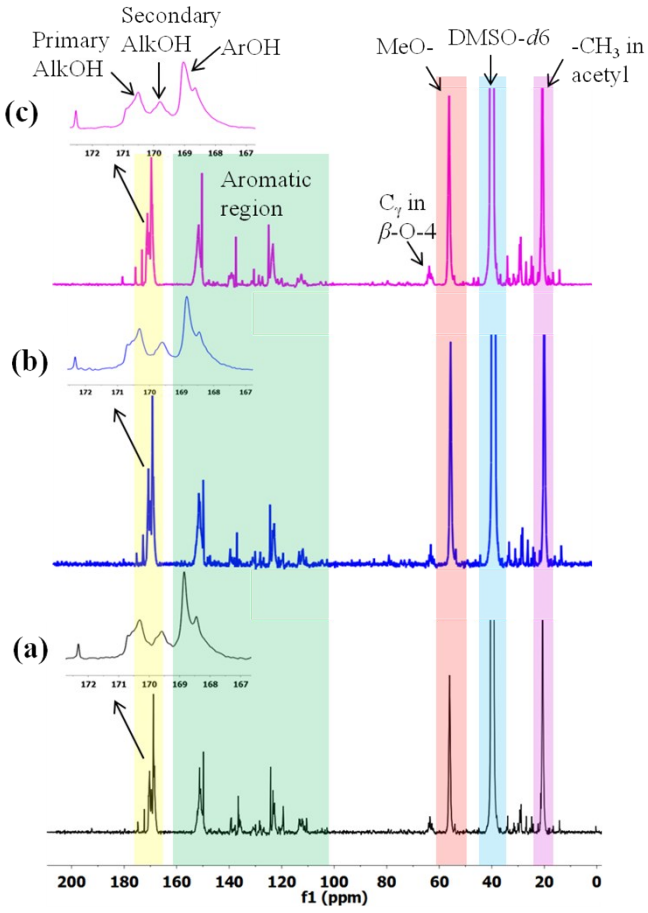


Fig. S1. $^{13}C$ NMR spectra of lignin. a, KL-Raw; b, KL-L/H-Insol.; c, KL-L/H-Sol. KL-Raw, raw Kraft lignin without laccase-HBT treatment; KL-L/H-Insol., water-insoluble fraction obtained from laccase-HBT (L/H) treatment of Kraft lignin; KL-L/H-Sol., water-soluble fraction obtained from laccase-HBT (L/H) treatment of Kraft lignin.

Table S1. The assignment and integration of $^{13}C$ NMR for lignin.

| Chemical shift (ppm) | Assignment | Number of moieties per aromatic ring | | |
|---|---|---|---|---|
| | | a | b | c |
| 172-169.6 | Primary aliphatic OH | 0.27 | 0.19 | 0.17 |
| 169.6-168.6 | Secondary aliphatic OH | 0.18 | 0.20 | 0.16 |
| 168.6-166 | Phenolic OH | 0.23 | 0.22 | 0.14 |
| 162-102 | Aromatic region | 1 | 1 | 1 |
| 57-54 | Methoxyl group | 0.65 | 0.93 | 0.81 |

**2D NMR Spectroscopy**

Lignin linkages were analyzed with heteronuclear single quantum coherence spectroscopy (HSQC). The acetylated lignin (150 mg) was dissolved in 1 mL of DMSO-*d6* and placed in the aforementioned NMR tube. Adiabatic 2D $^{1}H$-$^{13}C$ HSQC spectra were acquired on a Bruker AVANCE 500 MHz spectrometer as described by Mansfield et al (2012),[3] and the resultant data were processed with the software of Topspin version 3.2 (Bruker Biospin) with the following parameters: Gaussian apodization in F2 (LB = -0.5, GB = 0.001), and squared cosine-bell and forward linear prediction with 32 coefficients in F1.[3] The obtained HSQC spectra were then analyzed using software Sparky (https://www.cgl.ucsf.edu/home/sparky/), and the assignments of lignin linkages (I, II, III, and IV as shown in Fig. 1-e4) were shown in Table S2. These linkages were also presented in lignin oligomers (Fig. S2), among which I (*β*-*O*-4), II (*β*-5) and III (*β*-*β*) represented linear structures, and IV (5-5/*β*-*O*-4/*α*-*O*-4) had a branch structure. The chemical shifts of I*β* (*β* position in *β*-*O*-4), II*α* (*α* position in *β*-5) and III*α* (*α* position in *β*-*β*) were evaluated according to Tobimatsu et al (2013),[4] while chemical shift of IV*β* (*β* position in dibenzodioxocin) was evaluated according to Sette et al (2011)[5] and Crestini et al (2011).[6] For

quantification of these interunitery linkages in lignin, the well-resolved contours of I$\beta$, II$\alpha$, III$\alpha$, and IV$\beta$ (Fig. 1-e4) were integrated using the software MestReNova. The frequency of each linkage (% in Fig. 1-e1 to -e3) was calculated using the followed equation:[3]

$$Frequency\ (\%) = \frac{I_x}{I_{I\beta} + I_{II\alpha} + I_{III\alpha} + I_{IV\beta}} \times 100\ \%$$

Where $I_x$ is the integration of the linkage to be calculated, and $I_{I\beta}$, $I_{II\alpha}$, $I_{III\alpha}$, $I_{IV\beta}$ are the integrations of I$\beta$, II$\alpha$, III$\alpha$, and IV$\beta$, respectively. The above equation indicated that the quantified frequencies represented the relative changes in lignin linkages.

Table S2. Chemical shifts of lignin interunitery linkages.

| Linkages* | F2 (ppm) | F1 (ppm) |
|---|---|---|
| I$\beta$ | 6.0 | 74.5 |
| II$\alpha$ | 5.5 | 87.7 |
| III$\alpha$ | 4.5 | 87.0 |
| IV$\beta$ | 4.2 | 81.5 |

* Lignin linkages of I$\beta$, II$\alpha$, III$\alpha$, and IV$\beta$ are shown in Fig. 1-e4.

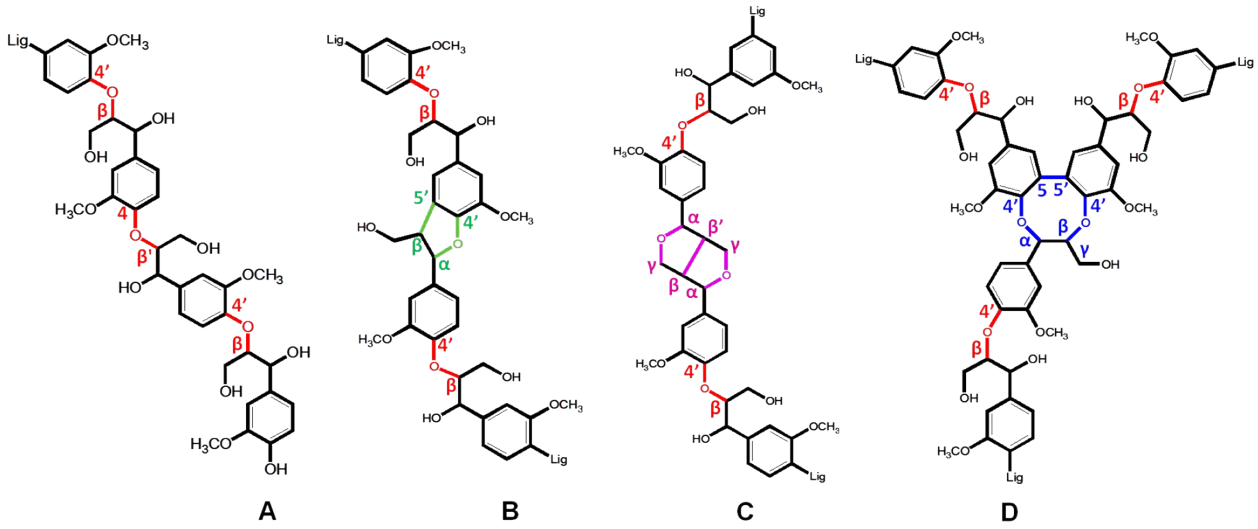


Fig. S2. Representative interunitery linkages in lignin structure. *β*-aryl ether (*β*-*O*-4) (A), phenylcoumaran (*β*-5) linked with *β*-*O*-4 moieties (B), and pinoresinol (*β*-*β*) linked with *β*-*O*-4 moieties (C) display linear structures. Non-phenolic dibenzodioxocin (5-5/*β*-*O*-4/*α*-*O*-4) linked with *β*-*O*-4 moieties (D) shows branchy structure. *β*-*O*-4, *β*-5, *β*-*β*, and dibenzodioxocin are highlighted in red, green, magenta, and blue, respectively. Lig- in the structures stands for lignin moieties.

**Gel Permeation Chromatography (GPC)**

GPC analysis was performed on an OMNISEC system (Malvern Instrument Ltd., Houston, TX). Two Styrene-divinyl benzene (SDVB) columns were used. Column temperature was set at 45 °C. DMF/0.02M Ammonium Acetate was used as the eluent at a flow rate of 1.0 mL/min. A viscometer and refractive index detector in the OMNISEC REVEAL system was used to measure the molecular weight. The acetylated lignin was dissolved in DMF at a concentration of 1 mg/mL, and 100 µL of the sample was injected into the GPC system after filtration with 0.45 µm membrane filter (VWR, Houston, TX). Universal calibration with poly(methyl methacrylate) standards were used. The data were processed with OmniSEC 5.12 software.

**Electrospinning**

Both lignin and PAN were grounded to fine powders and passed through 120-mesh screen. The lignin and PAN powders were then mixed at a weight ratio of 1:1 and dissolved in DMF to generate a 15 wt% solution, which was further loaded to a 10 mL syringe with a 22 gauge (i.d. 0.70 mm, length 38 mm) stainless steel blunt needle (Terumo, Yokohama, Japan). Lignin-PAN precursor fiber was produced using a nanofiber electrospinning unit (Kato Tech Co., Ltd., Kyoto, Japan). The syringe was placed in the syringe pump system in the unit, and the solution feed rate was set at 0.25 mL/h. The fiber was collected on aluminum foil. An electronic voltage of 11.5 kV for a uniform Taylor's cone was applied between the syringe needle and the aluminum disc. The distance between the syringe needle and the aluminum disc was kept at 17 cm to give a wagging stream and allow the solvent to be completely evaporated. The formed fibers were picked from the aluminum foil and kept in desiccator.

**Viscosity**

The dynamic viscosity of the electrospinning dopes was measured using Malvern Kinexus Pro+ rotational rheometer (Malvern Instruments, Houston, TX) with a 50 mm diameter parallel plate geometry. Sample thickness was 0.5 mm, and the tests were conducted at a constant temperature of 25 ºC with the shear rate from 600 $s^{-1}$ to 0.1 $s^{-1}$. Five data points were recorded per each decade of shear rate, and three measurements were replicated for each sample. The shear viscosity at 0.1 $s^{-1}$ shear rate was reported as the results. As shown in Fig. S3, pure PAN has much higher viscosity than all lignin/PAN blends.

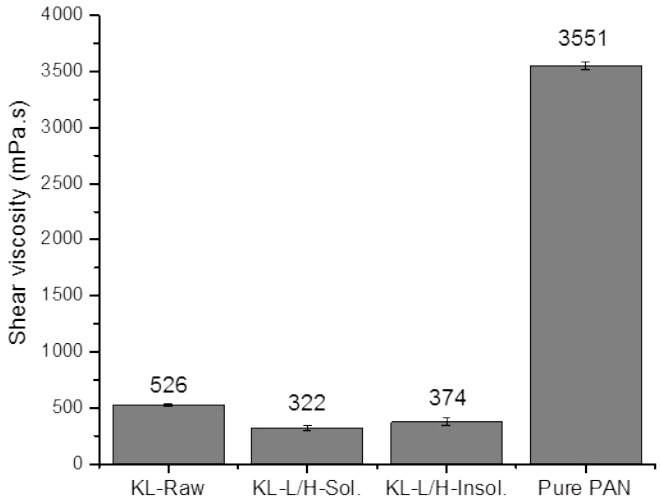


Fig. S3. Viscosity of lignin/PAN dopes at 0.1 $s^{-1}$ shear rate.

**Thermostabilization and carbonization of lignin precursor fibers**

Both thermostabilization and carbonization of lignin fibers were performed in a split tube furnace with vacuum system (GSL 1600X, MTI Corporation, Richmond, CA). The conditions for thermostabilization were: heating at atmosphere from room temperature to 250 $^{o}$C at a heating rate of 1 $^{o}$C/min. After holding for 1 h at 250 $^{o}$C, the furnace was automatically cooled down to room temperature. For carbonization, the thermostabilized fibers were put in the tube furnace, and the tube was then completely sealed. Before heating, the tube was purged with nitrogen gas for three times with vacuum pump purging until $1\times10^{-2}$ torr. The step was to ensure that no residual oxygen was left in the tube. The flow rate of nitrogen was kept at 240 ccm ($cm^3$/min) during heating. The temperature was increased from room temperature to 1 000 $^{o}$C with a heating rate of 5 $^{o}$C/min. The holding time at 1 000 $^{o}$C was 1 h. The yields of carbon fibers are shown in Table S3. The final yield of the insoluble lignin-based carbon fiber was slightly improved as compared to that of the raw lignin-based carbon fiber, whilst the soluble

lignin-based carbon fiber had slightly decreased yield when compared with untreated lignin-based carbon fiber.

Table S3. Yields (%) of carbon fibers.

| KL-Raw | KL-L/H-Sol. | KL-L/H-Insol. | Pure PAN |
|---|---|---|---|
| 42.8 | 38.3 | 45.0 | 42.4 |

%, based on the weight of as-spun fibers.

**Field emission scanning electron microscope (FE-SEM)**

The morphologies of carbon fibers were imaged using a FEI Quanta 600F FE-SEM (FEI Company, Hillsboro, OR). The samples were firstly coated with gold-palladium (10 nm thickness) using a Cressington 208 HR sputter coater (TED PELLA INC., Redding, CA). The working distance was 10 mm, and the accelerating voltage applied was 5 kV. The diameters of fibers were calculated using ImageJ software (https://imagej.nih.gov/ij/), by calculating at least 40 different carbon fibers.

SEM images of as-spun fibers made of lignin and PAN were shown in Fig. S4. In comparison with the fiber made of pure PAN (1567 nm, Fig. S4-D), all fibers derived from lignin/PAN blends (Fig. S4-A, -B, and -C) were much finer. The decrease in diameter of as-spun lignin-based fibers could be attributed to the decreased viscosity[7,8] when blending relatively low MW lignin (as shown in Fig. 1c) with high MW PAN (MW = 150 000 g/mol). In fact, the viscosity of pure PAN in DMF (15 w%) was 3551 mPa.s, which was deceased to 526 mPa.s when the PAN was blended with 50 % raw lignin (Fig. S3). In particular, when comparing insoluble lignin-based fiber (Fig. S4-C) with soluble lignin-based fiber (Fig. S4-B), the former had bead-free morphology and much more uniform diameters (60.4 % of fiber diameter

distributed within 601-800 nm). This could be due to three reasons: (a) the better miscibility of insoluble lignin with PAN (Fig. 3-a), (b) higher MW of insoluble lignin than soluble lignin to render higher viscosity of insoluble lignin/PAN dope (Fig. S3), (c) more linear molecule structure of insoluble lignin (Fig. S2A) to improve the interactions between lignin molecules and PAN chains.

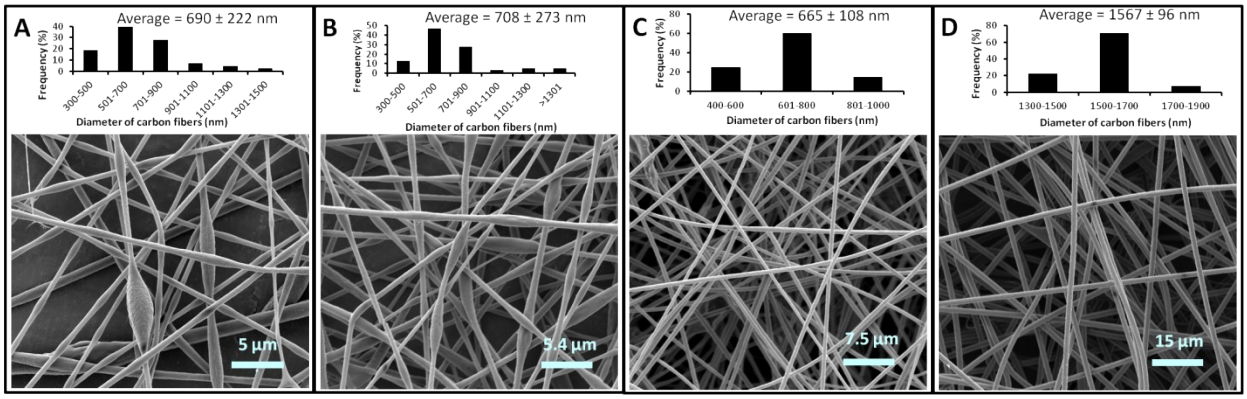


Fig. S4. SEM images of as-spun lignin fibers and PAN. A, KL-Raw; B, KL-L/H-Sol.; C, KL-L/H-Insol.; D, pure PAN. The upper histograms on each image were the distributions of carbon fiber diameters, measured with ImageJ® software for at least 40 different fibers.

**Differential scanning calorimetry (DSC)**

DSC was performed on the thermostabilized precursor fibers using DSC Q2000 system (TA Instruments, New Castle, DE) with three heating cycles. Three milligram of sample was placed in an aluminum pan. Under a nitrogen atmosphere, the samples were heated from room temperature to 350 $^{o}$C at the heating rate of 20 $^{o}$C/min. After cooling down to 0 $^{o}$C with a rate of 20 $^{o}$C/min, the second cycle and the subsequently third cycle were repeated at the same heating/cooling condition.

As shown in Fig. S5a, moisture and bonded water were started to be removed from the first cycle at about 80 °C as indicated of intensive endothermic peaks.[9] The decomposition temperature, as indicated by the onset of exothermic peaks (yellow region in Fig. S5a), suggested the onset of weight loss due to thermal decomposition of polymers in precursor fibers. This decomposition temperature was expressed as $T_{onset}$ and shown in Fig. S5b. The PAN precursor had a $T_{onset}$ at approximately 310 °C, at which the cyclization of PAN[10] and the cleavage of labile oxygen-containing groups[11] including the ether-linkages in lignin[12] probably happened.

The glass transition temperature ($T_g$) of precursor fibers, represented in Fig. 3a, was estimated from the second cycle as shown in Fig. S6.

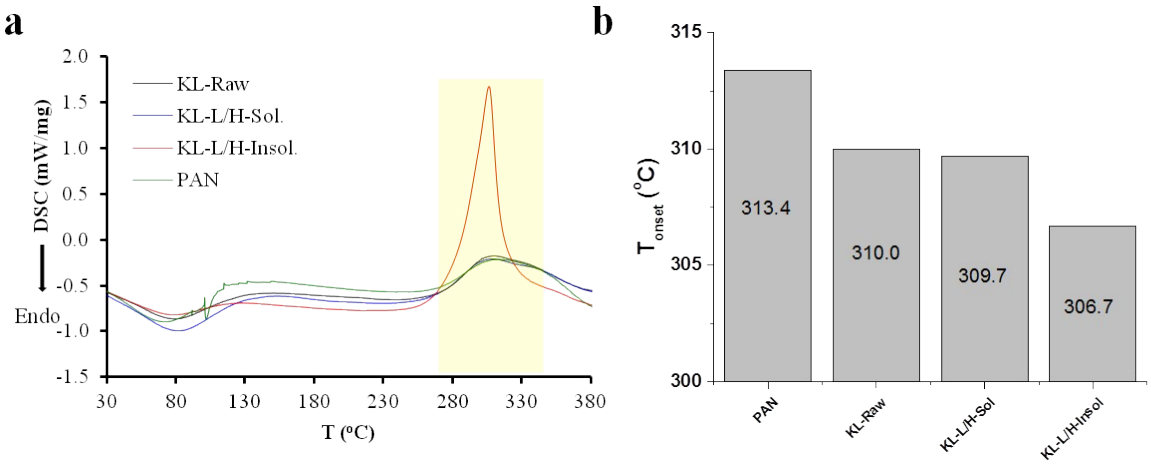


Fig. S5. First heating cycle of DSC analysis of thermostabilized precursor fiber (a), and the onset temperature ($T_{onset}$) derived from DSC (b).

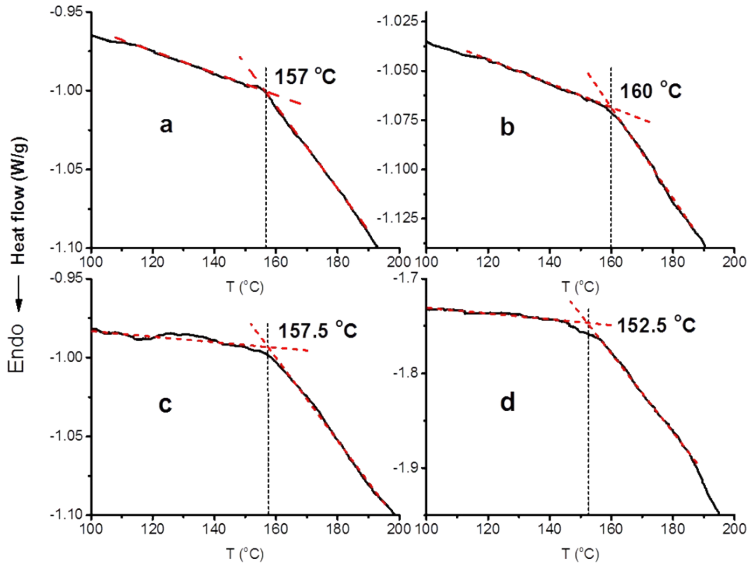


Fig. S6. $T_g$ of thermostabilized precursor fibers made of lignin/PAN composite and pure PAN. The heating flow curves were derived from the second heating cycle of DSC analysis. a, PAN; b, KL-Raw; c, KL-L/H-sol.; d, KL-L/H-insol..

**X-ray diffraction (XRD)**

The graphitic structure in carbon fibers was analyzed using Bruker D8 Discovery X-ray diffraction (Bruker, Madison, WI). X-ray resource was generated at 40 mA current and 40 kV voltage with Cu Ka wavelength (λ) of 1.542 Å. Diffractograms (Fig. S7a) were recorded in the 2θ range of 10°-50°. Scanning step size was set at 0.05°, and the scanning rate was 1.5°/min. The crystalline size ($L_{hkl}$) was calculated using Scherrer equation:

$$L = \frac{K\lambda}{\beta \cos\theta} \qquad \text{Equation (1)}$$

where $L$ is the crystalline size, nm; K is shape factor, set as 0.94 in this calculation; λ is the X-ray wavelength (1.542 Å); $\beta$ is the full width at half maximum (FWHM) in radian; $\theta$ is the Bragg angle in degree.

The distance between two crystalline lattices ($d_{hkl}$) was estimated using Bragg's law:

$$2d\sin\theta = n\,\lambda \qquad \text{Equation (2)}$$

where $d$ is distance in nm; $\theta$ is the Bragg angle in degree; n is set as 1. The results were shown in Fig. S7b. Diffractogram of commercial graphite and the calculated $L_{hkl}$ and $d_{hkl}$ were shown in Fig. S8.

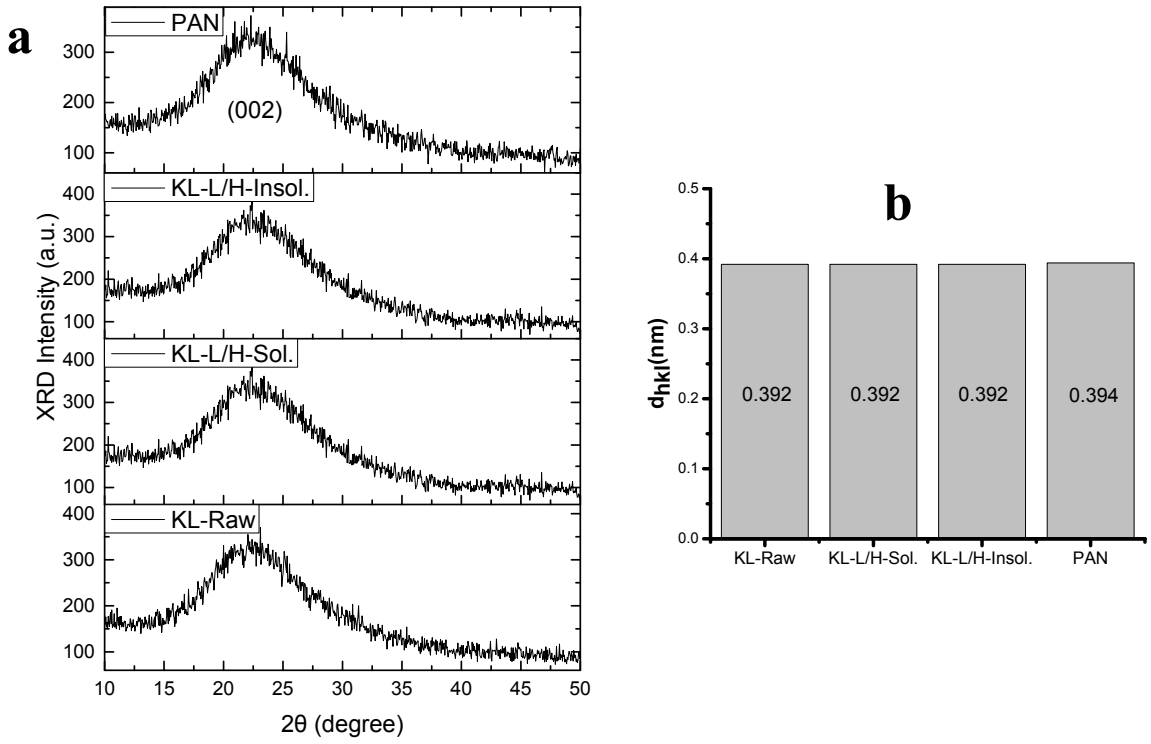


Fig. S7. XRD spectra of lignin and PAN (a), and the distance between two atomic layers in crystal structures as calculated with Bragg law (b).

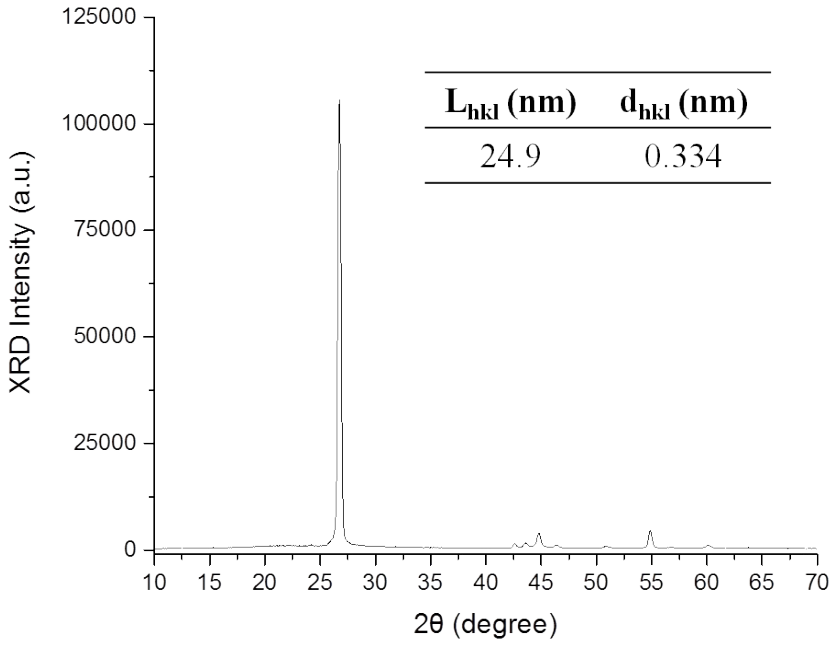


Fig. S8. XRD spectrum of commercial graphite powder. The inserted table shows the crystallite size ($L_{hkl}$) and the distance between crystallite interlayers ($d_{hkl}$).

**Raman spectroscopy**

For Raman spectroscopy, carbon fibers were briefly ground and then mounted on a double adhesive tape fixed on a glass slide. Raman spectra were taken using a Horiba Jobin-Yvon LabRam Raman Confocal Microscope system with 633 nm laser, 10× magnification of objective lens, D0.3 filter, 200 μm confocal pinhole, 10 s exposure time, and 3 accumulations. Guassian curve fitting was used with Origin 9 software to analyze the obtained Raman spectra. The Raman shift of D band and G band was confirmed by the commercial graphite, which shows D band at 1348 $cm^{-1}$, and G band at 1581 $cm^{-1}$ (Fig. S9a), and the measured Raman spectra were shown in Fig. S9b.

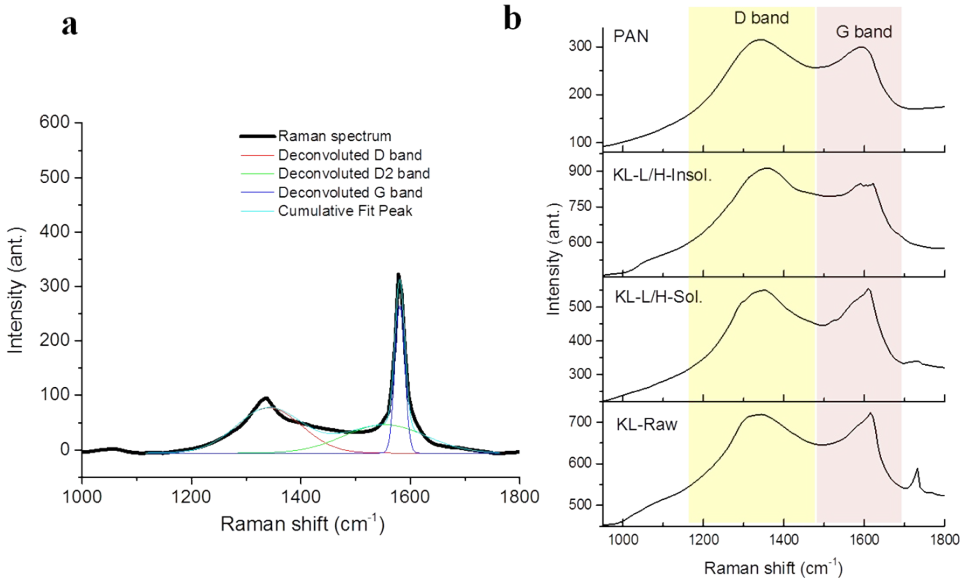


Fig. S9. Raman spectra of commercial graphite powder (a), and carbon fibers made from lignin and PAN (b).

**Thermogravimetric analysis (TGA)**

TGA measurement was carried out using a TA Instruments Q600-SDT system in a nitrogen gas environment (100 mL/min). Thermostabilized precursor fibers were placed in 90 μL alumina crucibles, and heated from room temperature to 1 000 °C with the heating rate of 10 °C/min. As shown in Fig. S10 and Table S4, the yield of carbon fiber made of water-insoluble lignin fraction and PAN at 1 000 °C degree was the slightly lower than the other three types of carbon fiber. The lower yield was consistent with higher *β-O*-4 linkages in lignin (Fig. 1-e), which begun to decompose at around 306 °C as shown in DSC spectra (Fig. S5a), and probably induced the significant weight loss before 450 °C as shown in Table S4.[9,12]

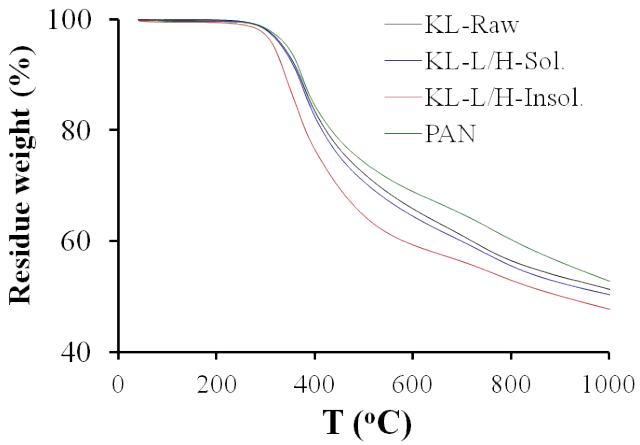


Fig. S10. TGA of thermostabilized carbon fiber precursors. KL-Raw, raw Kraft lignin without laccase-HBT treatment; KL-L/H-Insol., water-insoluble fraction obtained from laccase-HBT (L/H) treatment of Kraft lignin; KL-L/H-Sol., water-soluble fraction obtained from laccase-HBT (L/H) treatment of Kraft lignin.

Table S4. Residue weight (%) of carbon fiber during carbonization derived from TGA curves.

| | **150 °C** | **300 °C** | **450 °C** | **600 °C** | **950 °C** |
|---|---|---|---|---|---|
| PAN | 99.7 | 98.4 | 78.3 | 68.9 | 54.5 |
| KL-Raw | 99.8 | 98.2 | 76.7 | 65.8 | 52.5 |
| KL-L/H-Sol. | 100 | 98.1 | 75.3 | 64.4 | 51.3 |
| KL-L/H-Insol. | 99.5 | 97.1 | 69.6 | 59.3 | 48.9 |

**Nanoindentation**

Mechanical properties of resultant fibers were measured using Hysitron TI 950 Triboindenter (Minneapolis, MN). Before the measurement, carbon fibers were embedded in an epoxy resin

(Epofix™ embedding resin kit, Electron Microscopy Science, Hatfield, PA). The resin was polymerized in room temperature overnight. To get a smooth surface for nanoindentation, the resin was firstly polished by a RMC Boeckeler MTX microtome (Boeckeler Instruments Inc., Tucson, AZ) with diamond knife, and continued to polish with a EcoMet 3 grinder/polisher (Buehler, Lake Bluff, IL) using 0.3 μm Alfa alumina powder (Type DX, Electron Microscopy Science, Fort Washington, PA) until fibers can be clearly found on the epoxy resin surface under light microscope.

Nanoindentation was carried out on transverse section of fiber (Fig. S11) using a Cube Corner (90°) tip with 40 nm radius. The calibration of the tip for the area function was made prior the test by indenting a fused quartz standard sample. The indentation depth of the fibers was set at 15-20 nm to avoid the effects of substrate on the measurement.[13] For each sample, fifteen different indentations were conducted on three different carbon fibers. The reduced elastic modulus ($E_r$) was given as transverse modulus, which was obtained from the slope of initial unloading curve in loading-displacement ($P$-$h$) curve (Fig. S12) using the following equations:[14]

$$E_r = \frac{\sqrt{\pi}}{2\sqrt{A}} \times S \qquad \text{Equation (3)}$$

where $E_r$ is the reduced elastic modulus, $A$ is the contact area, and $S$ is the stiffness.

The stiffness ($S$) in Equation (3) is given by $S = \mathrm{d}P/\mathrm{d}h$ as shown in Fig. S12, which $P$ and $h$ are loading and displacement, respectively. The relationship between the reduced elastic modulus ($E_r$) and Young's modulus is shown in the equation (4).[14]

$$\frac{1}{E_r} = \frac{(1 - v_i^2)}{E_i} + \frac{(1 - v_s^2)}{E_s}$$

Equation (4)

Where $E_i$ and $E_s$ are the Young's modulus of indenter (1140 GPa) and sample respectively. $v_i$ and $v_s$ are the Poisson's ratio of indenter (0.07) and sample respectively. An improved reduced elastic modulus thus indicated a potential higher Young's modulus in macroscopic applications.

The hardness ($H$) was calculated as in equation (5):

$$H = \frac{P_{max}}{A} \quad \text{Equation (5)}$$

where $H$ is given as hardness, $P_{max}$ is the maximum force as shown in Fig. S12.

The calculated hardness of carbon fibers was shown in Fig. S13. Carbon fiber made of laccase-HBT treated lignin and PAN had increased hardness than carbon fiber made of untreated Kraft lignin, suggested their greater resistances to plastic deformation under indentation. However, pure PAN-based carbon fiber had the highest hardness, which could be attributed to its highest pre-graphitic carbon structure as revealed by Raman spectroscopy (Fig. 3b).

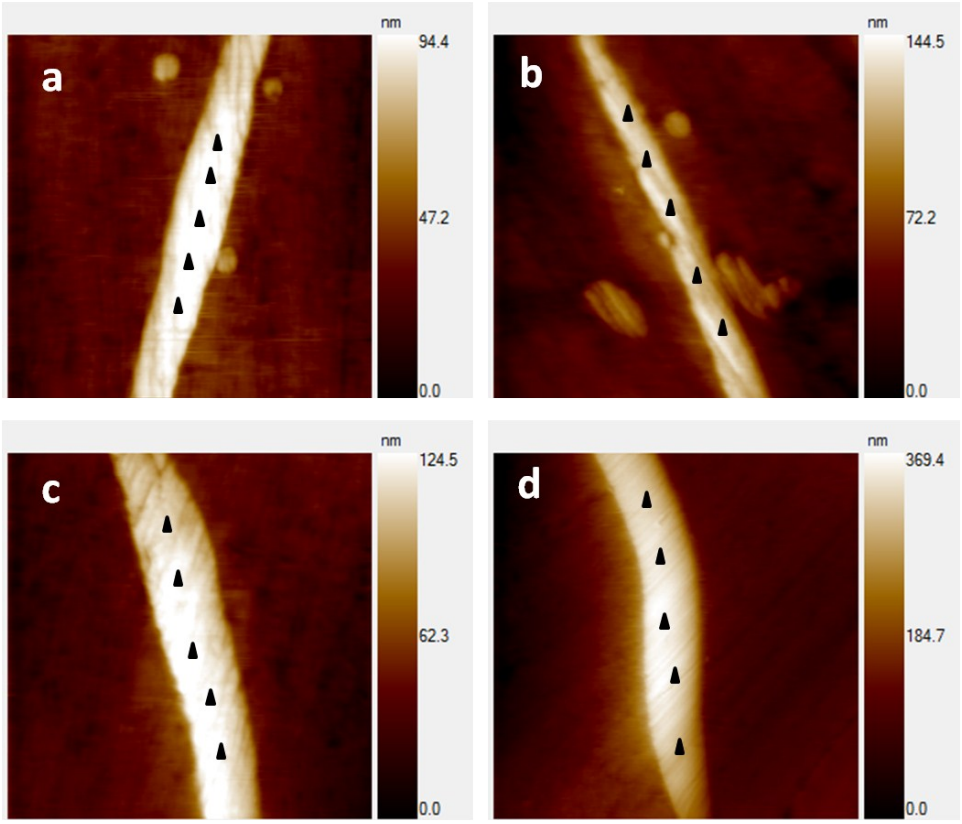


Fig. S11. Topography of scanning probe microscopy (SPM) under nanoindentation. a, KL-Raw; b, KL-L/H-soluble; c, KL-L/H-insoluble; d, PAN. Since the tip indents (15 nm depth) are too small to be visualized under our SPM, the positions for nanoindentations along the carbon fiber were indicated as mannually inserted solid triangles on the fibers.

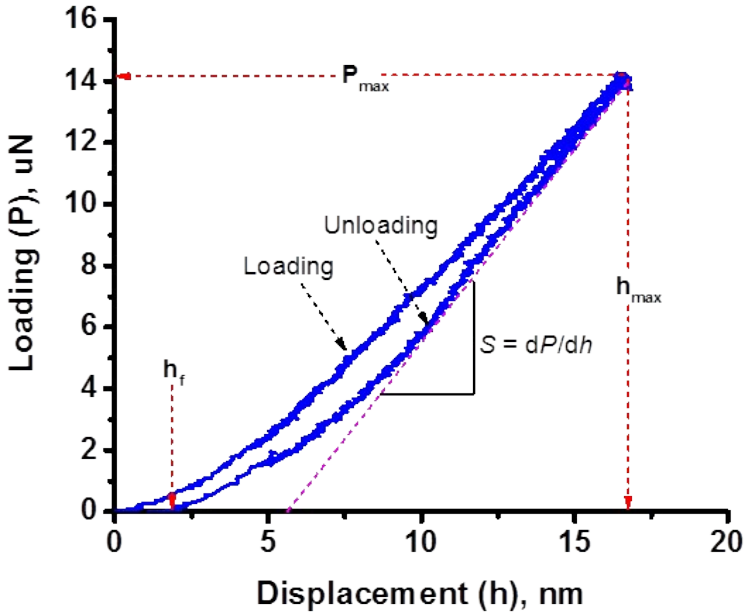


Fig. S12. An example of loading-displacement curve (KL-L/H-Insol.) from nanoindentation. $P_{max}$ is the maximum loading, $h_{max}$ is the maximum displacement, $h_f$ is the final displacement, $S$ is the stiffness. Plotting this figure was referred to Oliver and Pharr (1992).[14]

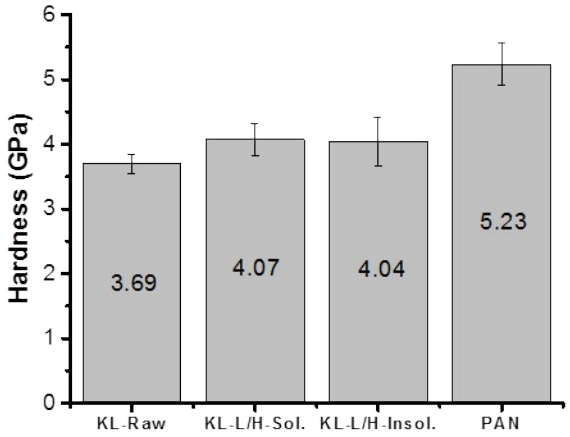


Fig. S13. The hardness of carbon fibers measured by nanoindentation.

Table S5. Comparison of the reduced elastic modulus of carbon fiber in this study with the published elastic modulus of commericial carbon fibers as measured by nanoindentation.

| Ref. | Carbon fiber | Vendor | Fiber precursor | Reduced modulus (GPa)* |
|---|---|---|---|---|
| | K637 | Mitsubishi | Pitch | 10.7 ± 3.1 |
| 13 | M40J | Toray | PAN | 15.0 ± 4.9 |
| | M46J | Toray | PAN | 14.0 ± 4.7 |
| 15 | M46J | Toray | PAN | ~14 GPa |
| 16 | T700SC | Toray | PAN | 23.17 ± 1.27 |
| 17 | Lignin micro-particles | Homemade | Kraft lignin | 8.2 ± 3.04 |
| Our research | | Homemade | Kraft lignin/PAN (Laccase-HBT) | 21.8 ± 1.3 |

* all reduced elastic modulus in this table were measured by nanoindentation at the transverse direction of carbon fibers.

**References**


1. C.-L. Chen. *In Methods in Lignin Chemistry*, (Eds: Lin, S. Y.; Dence, C. W.), Springer–Verlag, NY, USA 1992.
2. E. A. Capanema, M. Y. Balakshin, J. F. Kadla. *J. Agric. Food Chem.* 2005, **53**, 9639-9649.
3. S. D. Mansfield, H. Kim, F. Lu, J. Ralph. *Nat. Protocols* 2012, **7**, 1579-1589.
4. Y. Tobimatsu, F. Chen, J. Nakashima, L. L. Escamilla-Treviño, L. Jackson, R. A. Dixon, J. Ralph. *Plant Cell* 2013, **25**, 2587-2600.
5. M. Sette, R. Wechselberger, C. Crestini. *Chem. Eur. J.* 2011, **17**, 9529-9535
6. C. Crestini, F. Melone, M. Sette, R. Saladino. *Biomacromolecules* 2011, **12**, 3928-3935.
7. M. Ago, K. Okajima, J. E. Jakes, S. Park, O. J. Rojas, *Biomacromolecules* 2012, **13**, 918-926.
8. R. Ding, H. Wu, M. Thunga, N. Bowler, M. R. Kessler. *Carbon*, 2016, **100**, 126-136.
9. X.-Z. Tang, B. Yu, R. V. Hansen, X. Chen, X. Hu, J. Yang. *Adv. Mater. Interfaces* 2015, **2**, 1-7.
10. T. J. Xue, M. A. McKinney, C. A. Wilkie. *Polym. Degrad. Stab.* 1997, **3910**, 193–202.
11. L. Wang, X. Jia, Y. Li, F. Yang, L. Zhang, L. Liu, X. Rao, H. Yang. *J. Mater. Chem. A* 2014, **2**, 14940-14946.
12. T. Nakamura, H. Kawamoto, S. Saka. *J. Anal. Appl. Pyrolysis*, 2008, **81**, 173–182.
13. R. Maurin, P. Davies, N. Baral, C. Baley. *Appl. Comp. Mater.* 2008, **15**, 61-73.
14. W. C. Oliver, G. M. Pharr. *J. Mater. Res.* 1992, **7**, 1564-1583.
15. M. G. Huson, J. S. Church, A. A. Kafi, A. L. Woodhead, J. Khoo, J. Khoo, M.S.R.N. Kiran, J. E. Bradby, B. L. Fox. *Carbon*, 2014, **68**, 240-249.

16. Z. Fan, R. Tan, K. He, M. Zhang, W. Peng, Q. Huang. *Chem. Eng. J.* 2015, **272**, 12-16.

17. W. Gindl-Altmutter, C. Fürst, A. Mahendran, M. Obersriebnig, G. Emsenhuber, M. Kluge, S. Veigel, J. Keckes, F. Liebner. *Carbon* 2015, **89**, 161-168.